New Journal of Physics
The open access journal at the forefront of physics

Deutsche Physikalische Gesellschaft DPG
IOP Institute of Physics

Published in partnership with: Deutsche Physikalische Gesellschaft and the Institute of Physics

OPEN ACCESS

RECEIVED
21 August 2015

REVISED
28 October 2015

ACCEPTED FOR PUBLICATION
3 November 2015

PUBLISHED
7 December 2015

PAPER

Lagrangian description of Brillouin scattering and electrostriction in nanoscale optical waveguides

Vincent Laude and Jean-Charles Beugnot

Institut FEMTO-ST, Université de Franche-Comté, CNRS 15B avenue des Montboucons, F-25030 Besanon Cedex, France

E-mail: vincent.laude@femto-st.fr

Keywords: Brillouin scattering, electrostriction, optical forces

Abstract

The diffraction of light by sound waves is known as Brillouin scattering. In optical waveguides, Brillouin scattering can arise from both bulk contributions, modelled by photoelasticity, and surface contributions, which are due to the waveguide boundaries being shaken by propagating sound. The reciprocal effect, electrostriction, governs the coherent generation of sound by light. The bulk photoelastic contribution to Brillouin scattering is generally nonlinear but can be limited to a first-order expansion for small strain. We investigate the moving-interface contribution to Brillouin scattering in optical waveguides and show that it is also inherently nonlinear, leading to multi-phonon processes for large deformations. Limiting the perturbation to first order, we form a Lagrangian describing the interaction of sound and light. The Lagrangian contains both surface and bulk contributions to Brillouin scattering and electrostriction, and allows the derivation of optical and acoustic equations in a single variational formula. A full electrostriction equation is then derived for the phonon distribution, with both bulk and surface effects included. Numerical simulations in the case of a silicon nanowire illustrate the different effects and their respective contributions.

1. Introduction

Brillouin scattering in a transparent medium occurs when light interacts coherently with spatio-temporal periodic variations of the refractive index caused by the propagation of sound waves [1]. The result of the interaction is that a fraction of the transmitted light wave changes its frequency and wavenumber, as if it were diffracted by an oscillating and moving grating. In bulk dielectric media, this interaction is described by the photoelastic effect. Reciprocally, the coherent mixing of two optical waves with different frequency and wavenumber produces mechanical force-like action on the propagation medium, or electrostriction, that generates sound within it. The pair of reciprocal physical mechanisms, photoelasticity and electrostriction, classically forms the basis for the description of stimulated Brillouin scattering (SBS), a nonlinear process by which light interacts coherently with acoustic vibrations in an optically transparent medium and energy can be transferred back and forth between them [2].

Light and sound interaction in microstructured optical fibres [3], microwires [4], and nanoscale waveguides [5–8] has attracted a lot of attention in recent years, due to the realization that surface effects can contribute significantly to the interaction. Rakich *et al* have shown that radiation pressure can indeed contribute significantly to the SBS gain in nanoscale optical waveguides [9, 10], allowing one in principle to design slot optical waveguides where this gain can be maximized [11]. These developments parallel the field of opto-mechanical interactions in cavities [12], including sound and light interaction in simultaneous photonic and phononic, or phoxonic, crystal structures [13]. In particular, the important role played by moving interfaces or surfaces in the coupling between light and sound has now been recognized and its complementarity with the bulk photoelastic effect is well understood [14, 15].

In this paper, we wish to precise in more detail the surface and bulk contributions to electrostriction, but also the reciprocity between the moving-interface (MI) effect and radiation pressure. We first summarize the method

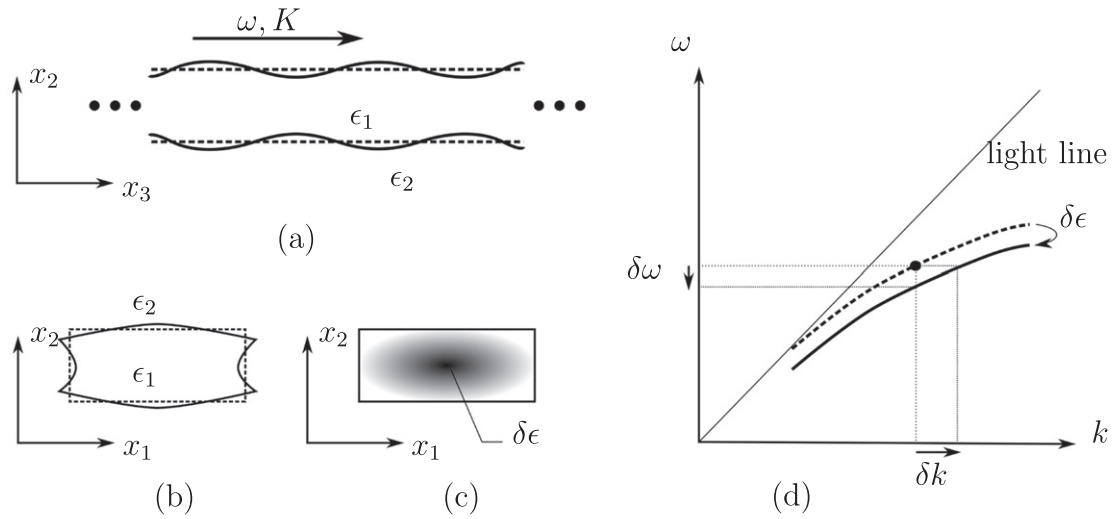

Figure 1. Propagation of an acoustic wave in an optical waveguide and its effect on optical properties. (a) An acoustic wave propagates along the waveguide, causing both a modulation of the dielectric tensor around its static value ϵ_1 and a deformation of the boundaries of the waveguide. (b) Indeed, at each position along the waveguide, the cross-section of the waveguide appears to be modulated geometrically: each point of the boundary is shifted by the normal displacement $\boldsymbol{u}(t, \boldsymbol{x})$. (c) Concurrently, at each point $\boldsymbol{x}$ inside the waveguide, the dielectric tensor is perturbed by an amount proportional to the strain field accompanying the acoustic wave, the so-called photoelastic effect. Both basic mechanisms (b) and (c) contribute to coupling of light and sound in the waveguide. (d) As a result, the dispersion relation of guided optical waves $\omega(k)$ is modulated in time at the acoustic frequency Ω.

of overlap integrals as applied to estimating coupling coefficients between optical and acoustic modes, before discussing the contribution of the MI effect to Brillouin scattering in optical waveguides. We had previously accounted for bulk electrostriction in optical fibres [16] and waveguides [17], excluding surface effects. Here, we show that the MI effect provides a natural way to describing radiation pressure as its reciprocal process in an interaction Lagrangian. Finally, we show that the total Lagrangian containing both surface and bulk contributions to Brillouin scattering and electrostriction leads to an elastodynamic equation for the generation of sound by light.

2. Theory

The usual approach to estimating quantitatively the interaction of light and sound in an optical fibre or waveguide is to express coupling coefficients involving overlap integrals of guided optical waves with acoustic waves; we summarize briefly known results in section 2.1. Sections 2.2 and 2.3 contain our main original developments.

2.1. Overlap integrals

Let us consider a dielectric optical waveguide, as depicted by figure 1. Guided optical waves satisfy a dispersion relation relating their frequency ω and wavenumber, or propagation constant, k. This dispersion relation is determined by the spatial distribution of the dielectric constant, or more generally the dielectric tensor ϵ for anisotropic media. Such a structure also supports the propagation of acoustic waves, in the form of elastic waves in solids [18].

Coupling coefficients can be obtained if the originally unperturbed optical and acoustic waves can be assumed to be known. It seems indeed grounded to write the total electric field as a superposition $\boldsymbol{E} = \boldsymbol{E}^{(1)} + \boldsymbol{E}^{(2)}$ of 2 guided modes involved in the acousto-optical interaction. More precisely, each guided mode ($\alpha = 1, 2$) is written

$$\boldsymbol{E}^{(\alpha)}(t, \boldsymbol{x}) = a^{(\alpha)}\left(t, x_3\right)\boldsymbol{e}^{(\alpha)}\left(x_1, x_2\right)\exp\left(\imath\left(\omega^{(\alpha)}t - k^{(\alpha)}x_3\right)\right) + \text{c.c.} \tag{1}$$

The a^{α} are modal amplitudes and the modal shapes $\boldsymbol{e}^{(\alpha)}$ can be obtained from the eigenvalue problem defining the dispersion relation.

We also write the displacements of the acoustic wave as

$$\boldsymbol{u}(t, \boldsymbol{x}) = \boldsymbol{u}\left(x_1, x_2\right)\exp\left(\imath\left(\Omega t - Kx_3\right)\right) + \text{c.c.} \tag{2}$$

This equation implies that the acoustic wave has a definite frequency Ω and a wavenumber K. Actually, the phase-matching conditions $\Omega = \omega^{(2)} - \omega^{(1)}$ and $K = k^{(2)} - k^{(1)}$ are assumed to hold exactly. In other words, among all possible phonons in the waveguide, we consider only those that satisfy the conditions for Stokes Brillouin scattering. It should not be concluded, however, that the acoustic wave is a particular elastic mode of the waveguide structure. Indeed, the waveform $\boldsymbol{u}(x_1, x_2)$ in (2) remains in principle arbitrary, as long as it satisfies the elastodynamic equations.

As depicted in figure 1, acoustic waves modulate both the dielectric tensor of the medium and the boundaries of the waveguide. This modulation in time is small and it can be considered as a perturbation. Considering the optical dispersion relation, the perturbation induces a change in the modal frequency at fixed wavenumber, but also a change in the modal wavenumber at fixed frequency. These can be characterized by the relative modulations $\delta\omega/\omega$ or $\delta k/k$. They are related by $\delta k = -(v_g)^{-1}\delta\omega$ where v_g is the group velocity [19, 20], as figure 1(d) illustrates.

Assuming that the acoustic wave is known, coupling coefficients can then be computed from overlap integrals (see also Appendix B). Note that we specifically assume vanishing optical loss in this paper. The bulk contribution to the acousto-optical effect comes from the photoelastic effect and leads to [13]

$$\left(\frac{\delta\omega}{\omega}\right)_{\mathrm{PE}} = \frac{1}{2}\int_S \mathrm{d}S\; p_{ijkl}\, d_i^{(1)} d_j^{(2)*} u_{k,l}, \tag{3}$$

where we have assumed the optical modes are normalized such that $\int_S \mathrm{d}S\; \boldsymbol{e}^{(\alpha)*}\cdot\boldsymbol{d}^{(\alpha)} = 1$, with S the cross-section of the waveguide. In these expressions, $\boldsymbol{d}^{(\alpha)}$ is the dielectric displacement vector of mode α and p_{ijkl} is the photoelastic tensor. We use tensor notations: repeated index summation is implied and an index placed after a coma indicates a spatial partial derivative, i.e. $u_{k,l} = \frac{\partial u_k}{\partial x_l}$. It should be noted that the strain tensor field $u_{k,l}$ includes both partial derivatives with respect to x_1 and x_2 and a term proportional to K. The later contribution is absent from the similar formula for phoxonic and optomechanical cavities [21]. As a note, expression (3) is limited to the first-order term in a nonlinear expansion of the relative dielectric tensor with strain. Higher-order nonlinear terms are not considered in this paper.

The surface contribution to the acousto-optical effect comes from the MI effect and can be given the form of a contour integral [13, 19]

$$\left(\frac{\delta\omega}{\omega}\right)_{\mathrm{MI}} = -\frac{1}{2}\int_\Sigma \mathrm{d}l\; u_n \left(\Delta\epsilon\; \boldsymbol{e}_t^{(1)}\cdot\boldsymbol{e}_t^{(2)*} - \Delta\epsilon^{-1}\, d_n^{(1)} d_n^{(2)*}\right), \tag{4}$$

with $\Delta\epsilon = \epsilon_1 - \epsilon_2$ and $\Delta\epsilon^{-1} = \epsilon_1^{-1} - \epsilon_2^{-1}$. In this expression, u_n is the normal displacement at the interface Σ between the waveguide and the surrounding medium, so that $(\mathrm{d}l\, u_n)$ represents the change in the cross-sectional area of the waveguide as the acoustic wave is propagating. Significantly, the electromagnetic (EM) field has been decomposed into normal and tangential components, so that only components that are continuous across the interface Σ are involved. As argued by Johnson *et al*, such a formula applies only within the frame of first-order perturbation theory applied to the variation of the dielectric tensor [19]. It remains that there may well be perturbation terms other than the linear one to be taken into account, as investigated next. As a final note, mode labels were not explicited in the left-hand sides of expressions (3) and (4) because only backward intra-mode Brillouin scattering will be considered in the following examples, but they should in general be indicated if the two optical modes differ.

2.2. Moving interfaces

As shown in the case of multilayers [14], and 2D [22] and 3D [21] cavities, the MI effect can be investigated adequately under an quasi-static approximation. We here extend this approach to waveguides. Let us consider the guided optical mode equation written for the electric field vector

$$\nabla\times\left(\frac{1}{\mu}\nabla\times\boldsymbol{E}\right) + \frac{\partial^2(\epsilon\boldsymbol{E})}{\partial t^2} = 0. \tag{5}$$

If the waveguide is perfectly still, the dielectric tensor ϵ is a definite function of the transverse coordinates x_1 and x_2, and the equation can be solved to obtain propagation modes respecting appropriate boundary conditions. Now if an acoustic wave is present, it will modulate the dielectric tensor in time by adding to it a perturbation $\delta\epsilon_{ij} = \chi_{ijkl}u_{k,l}$ proportional to the strain field[1]. This modulation is, however, on the time scale of the acoustic wave and is thus very slow compared to the characteristic optical time (by a factor of 10^5 slower, approximately). We can thus imagine that the waveguide is quasi-statically modulated in time and that equation (5) can be solved for at every particular moment along the acoustic evolution to give the instantaneous optical modes and frequencies. Furthermore, because of the presence of the acoustic wave, the boundaries of the optical waveguide are also modulated in time. Each point $\boldsymbol{x}$ of the boundaries moves around its static position by an amount $\boldsymbol{u}$, according

[1] Note that the nonlinear tensor χ_{ijkl} is related to the photoelastic tensor by the relation $\chi_{ijkl} = -\epsilon_{im}\epsilon_{jn}p_{mnkl}$ [23].

to the displacement expressed by (2). We can safely ignore the longitudinal motion of the boundaries, as long as the displacements of the acoustic wave are very small compared to the acoustic wavelength, so that every cross-section of the waveguide can be thought of as 'breathing' slowly in time, at the acoustic frequency. In a practical numerical implementation, the motion of the interfaces can be incorporated in the mesh used to define the waveguide, as will be performed in section 3.1. Let us remark that such a computation will result in a function of time $(\delta\omega/\omega)_{\mathrm{MI}}(t)$ that naturally includes the full perturbation caused by the acoustic wave, as opposed to only the perturbation at frequency Ω in (4).

2.3. Lagrangian approach

As we argued in the introduction, our main goal is to formulate a variational principle from which both Brillouin light scattering by phonons and electrostriction of acoustic phonons by light can be derived simultaneously. As both elastodynamic and Maxwell's equations can be formulated using Lagrangians, we investigate how a total Lagrangian can be derived. In the context of our study, a Lagrangian is a functional depending on a vector field φ_i and its derivatives $\varphi_{i,j}$ with respect to time and spatial coordinates. Integrated over time, the Lagrangian defines the action of the system, which we seek to make stationary. We define the Lagrangian density as $\mathcal{L}(\varphi_i, \varphi_{i,j})$ so that the Lagrangian is the volume integral of this density, $L(\varphi_i, \varphi_{i,j}) = \int \mathrm{d}V\ \mathcal{L}(\varphi_i, \varphi_{i,j})$. The Euler–Lagrange equations are

$$\frac{\partial \mathcal{L}}{\partial \varphi_i} = \frac{\partial}{\partial x_j}\frac{\partial \mathcal{L}}{\partial \varphi_{i,j}}, \tag{6}$$

where summation over j is implicit (the index j runs over time t and coordinates x_j in this equation). The Euler–Lagrange equations yield the dynamical equations for the system.

For elastic waves, the Lagrangian density is well known to be [24]

$$\mathcal{L}_{\mathrm{e}} = \frac{1}{2}\left(\rho \dot{u}_i \dot{u}_i - c_{ijkl} u_{i,j} u_{k,l}\right), \tag{7}$$

with c_{ijkl} the tensor of elastic constants and ρ the mass density. This is the kinetic energy density minus the potential energy density. The elastic Lagrangian density depends only on the partial derivatives of the displacements with respect to time and space coordinates—velocities $\dot{u}_i$ and strains $u_{k,l}$. From a Legendre transform, the Hamiltonian density is simply $\mathcal{H}_{\mathrm{e}} = \frac{1}{2}(\rho \dot{u}_i \dot{u}_i + c_{ijkl} u_{i,j} u_{k,l})$, which is also the total energy density for elastic waves. Note that expression (7) is formally valid for lossless elastic wave propagation; the generalized Euler–Lagrange equations for the case of loss are given in Appendix C.

For EM waves and the microscopic formulation of Maxwell's equations, the Lagrangian is known to be given by [25]

$$\mathcal{L}_{\mathrm{o}} = -\rho_{\mathrm{e}}\phi + \boldsymbol{j}\cdot\boldsymbol{A} + \frac{1}{2}\left(\epsilon_0 E^2 - B^2/\mu_0\right), \tag{8}$$

where the potentials $(\phi, \boldsymbol{A})$ are used to express the electric field and the magnetic field vectors as

$$\boldsymbol{B} = \nabla \times \boldsymbol{A}, \tag{9}$$

$$\boldsymbol{E} = -\nabla\phi - \dot{\boldsymbol{A}}. \tag{10}$$

The source terms ρ_{e} and $\boldsymbol{j}$ account for charge and current density distributions. It is important to notice that the independent variables are the potentials, not the electric and magnetic fields, which are derived. For the macroscopic formulation of Maxwell's equations in dielectric media, the previous Lagrangian density can be rewritten as

$$\mathcal{L}_{\mathrm{o}} = \frac{1}{2}(\boldsymbol{E}\cdot\boldsymbol{D} - \boldsymbol{B}\cdot\boldsymbol{H}), \tag{11}$$

where the usual definitions $\boldsymbol{D} = \epsilon\boldsymbol{E}$ and $\boldsymbol{H} = \boldsymbol{B}/\mu_0$ are used. The dielectric displacement $\boldsymbol{D}$ in particular accounts for bound charges and currents. Under this form, the EM Lagrangian density still depends only on the partial derivatives of the potentials with respect to time and space coordinates. From a Legendre transform, the Hamiltonian density is simply $\mathcal{H}_{\mathrm{o}} = \frac{1}{2}(\boldsymbol{E}\cdot\boldsymbol{D} + \boldsymbol{B}\cdot\boldsymbol{H})$, which is also the total energy density for EM waves. For convenience, these relations are briefly derived in Appendix A. Note again that we specifically assume vanishing optical loss.

In order to describe Brillouin scattering in the optical waveguide, we propose to sum the EM and the elastic Lagrangians to form a total Lagrangian for the waves in interaction. This procedure is justified by the possibility to use a double Legendre transform to transform this total Lagrangian to a total Hamiltonian, so that the total energy of the system is taken into account in the interaction. As implied by the discussion in sections 2.1 and 2.2, and within the quasi-static approximation, the low-frequency variations of the EM energy originate solely from the variations of the dielectric tensor caused by the acoustic wave. We consequently separate the dielectric tensor

into its unperturbed and its first-order parts to write

$$L = L_o + L_e + \frac{l_3}{2}\int_S \mathrm{d}S\chi_{ijkl}E_iE_ju_{k,l} + \frac{l_3}{2}\int_\Sigma \mathrm{d}l\ u_n\left(\Delta\epsilon\left|\boldsymbol{E}_\parallel\right|^2 - \Delta\epsilon^{-1}D_\perp^2\right), \tag{12}$$

with l_3 some axial length introduced to write the integration volume as $V = l_3 S$, $L_o = \int \mathrm{d}V\ \mathcal{L}_o$, and $L_e = \int \mathrm{d}V\ \mathcal{L}_e$. We have further intentionally separated the bulk and the surface contributions in the first-order part. The surface integral accounts for the bulk photoelastic effect, while the contour integral accounts for the moving interface effect. It can be seen that the coupling coefficients (3) and (4) can be directly derived from them by inserting the optical modal superposition (1) and the acoustic waveform (2), and then keeping only terms at the acoustic frequency Ω. The validity of the moving interface Lagrangian is as before limited to the conditions of application of first-order perturbation theory.

Taking the variation of the total Lagrangian (12) with respect to the EM potentials, we are led back to the dynamical equation (6), including the photoelastic effect. The variation of the contour integral specifically leads to an expression of the MI effect as a boundary condition to the optical waveguide equation, combining the incident optical wave and the acoustic wave displacements at the interface Σ. The procedure we outlined in section 2.2 is actually a variant where the waveguide geometry is deformed at each time step within the acoustic period instead of modifying the boundary conditions.

The previous observations are intended to emphasize the consistency of the Lagrangian approach, but its real usefulness reveals in the description of electrostriction. We can indeed reinterpret the contour integral in (12) as the work done by the boundary of the waveguide when subjected to a surface optical force, or optical pressure, defined by

$$F_s = \frac{1}{2}\left(\Delta\epsilon\left|\boldsymbol{E}_\parallel\right|^2 - \Delta\epsilon^{-1}D_\perp^2\right). \tag{13}$$

Following [16] we further define an electrostriction stress tensor as $T_{ij}^{es} = \frac{1}{2}\chi_{klij}E_kE_l$. With these definitions, the dynamical equations for the elastic wave are derived using the Euler–Lagrange equations as

$$\rho\ddot{u}_i - \frac{\partial}{\partial x_j}\left(c_{ijkl}u_{k,l}\right) + \frac{\partial}{\partial x_j}T_{ij}^{es} = 0, \tag{14}$$

complemented with the boundary condition that the optical pressure F_s applies on every boundary where the dielectric tensor is discontinuous. The physical meaning of this equation is that the elastodynamics of the waveguide are forced by the combination of a bulk electrostriction stress distribution and of an electrostriction pressure, both of purely optical origin. As we illustrate in section 3.2, this formulation allows one to obtain the acoustic phonon distribution generated by light including both bulk and surface contributions to electrostriction.

3. Numerical results

Let us consider the simple rectangular silicon nanowire depicted in figure 2. The refractive index of silicon at a wavelength in a vacuum of 1550 nm is taken as $n = 3.48$ and refractive index dispersion is neglected. With a cross-sectional area $S \approx 0.1\ \mu\mathrm{m}^2$, this waveguide supports a fundamental TE mode with effective index $n_{\mathrm{eff}} = kc/\omega \approx 2.24$ and group index $n_g = c/v_g \approx 4.5$. As can be noticed from figure 2, the optical mode extends significantly in air around the central core. This situation is specifically chosen so as to maximize surface over bulk effects in Brillouin scattering, following Rakich's analysis [9, 10]. The chosen dimensions are also close to those used in Van Laer's experiments [8].

3.1. Quasi-static MI effect

Let us consider first the direct numerical simulation of the moving interface effect that we outlined in section 2.2. We consider specifically backward intra-mode Brillouin scattering, so that $K \approx 2k^{(1)}$, with the implication that the acoustic wavelength is half the effective optical wavelength. The silicon nanowire supports a total of 29 elastic modes with frequencies ranging between 12 and 30 GHz, and of course many more above. For each of these modes, normalized so that $L_e = 0.1$ J (with $l_3 = 1$ m), 24 snapshots were created within an acoustic period and the variation of the fundamental TE optical mode was recorded. As an illustration, figure 3 displays the optical mode at 4 different times ($t = 0, T/4, T/2, 3T/4$) with T the acoustic period, for the second and the third elastic modes. These elastic modes have very close frequencies, about 13.7 and 13.8 GHz respectively, but the former is of a rotational type while the latter is of the symmetric flexural type. The maximum total displacement and the symmetries of elastic modes are listed in table 1.

Different elastic modes actually have a quite different impact on the variations of the optical frequency. These variations are plotted in figure 4 for the previous two elastic modes, plus those with numbers 4 and 6. For

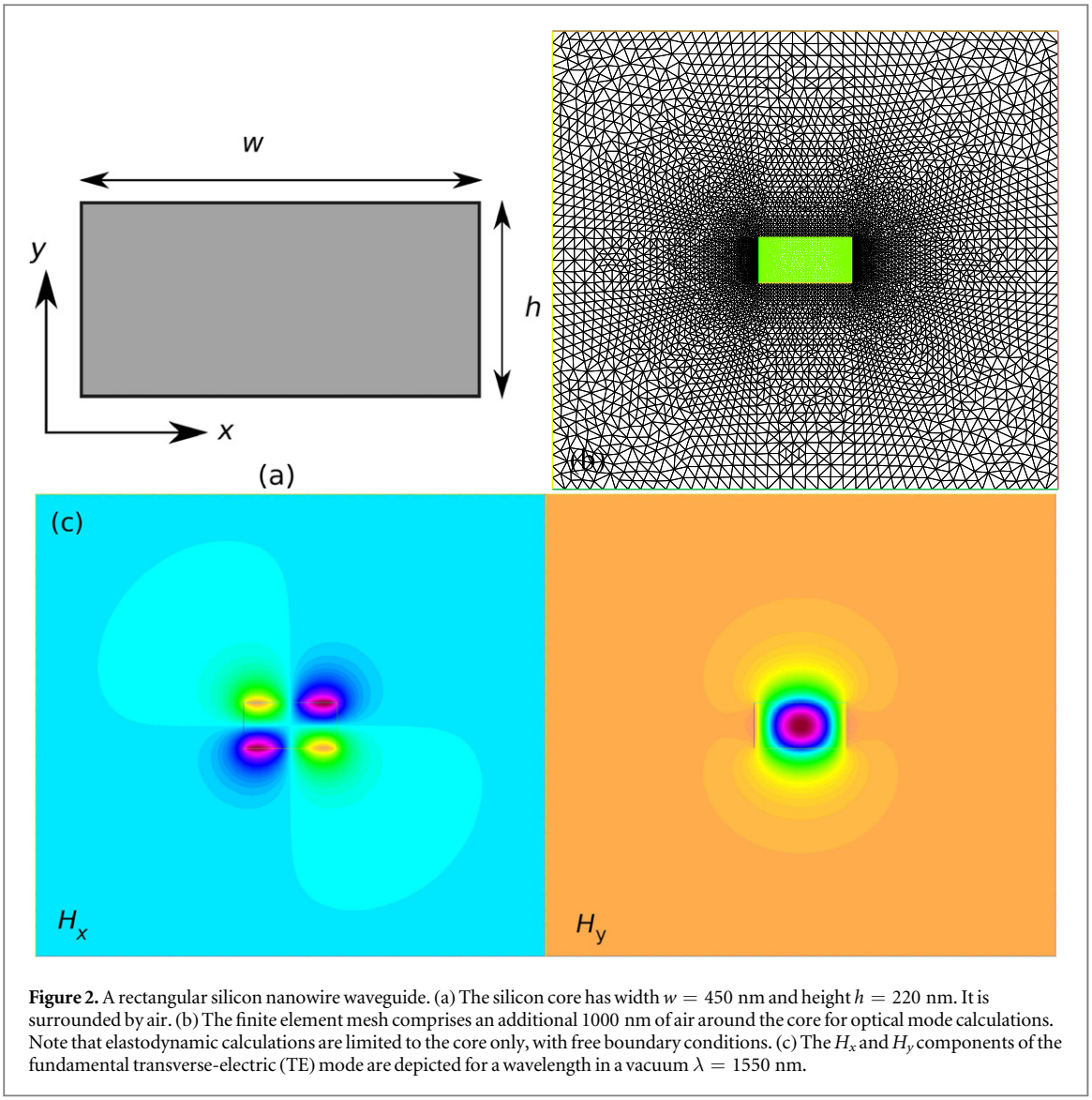

Figure 2. A rectangular silicon nanowire waveguide. (a) The silicon core has width $w = 450$ nm and height $h = 220$ nm. It is surrounded by air. (b) The finite element mesh comprises an additional 1000 nm of air around the core for optical mode calculations. Note that elastodynamic calculations are limited to the core only, with free boundary conditions. (c) The H_x and H_y components of the fundamental transverse-electric (TE) mode are depicted for a wavelength in a vacuum $\lambda = 1550$ nm.

each of them, the plot shows the value of $(\delta\omega / \omega)$ as caused by the MI effect and the photoelastic effect. The MI value is obtained from the previously described method, while the PE value is obtained directly from coefficient (3). Elastic modes 3 and 6 show rather strong MI and PE modulations, with similar amplitude and the same phase. The MI modulation is mostly sinusoidal at the frequency Ω of the elastic mode. In contrast, elastic modes 2 and 4 show a very small PE modulation and a small MI modulation. Moreover, the PI modulation is mostly at the double frequency 2Ω. Following the analysis by Psarobas *et al*, the acousto-optical response of the waveguide is nonlinear and is the siege of multi-phonon processes [14]. It must be stressed that this nonlinearity originates here solely from the MI effect and is of geometrical origin, since the PE effect was explicitly considered to be linear in expression (3). It is dependent on the acoustic mode energy: it was checked that diminishing the elastic mode energy by a factor of 2, the MI response was linearly decreased for elastic modes 3 and 6, while it was decreased by roughly a factor 4 for elastic modes 2 and 4. This is consistent with the fact that two-phonon processes are dominant in the latter case. Note that the vanishing of the linear PE and MI effects can be traced back to the symmetry properties of the considered elastic mode [26].

Finally, figure 5 shows the absolute values of the PE and MI modulation coefficients estimated using formulas (3) and (4) for all 29 elastic modes. It must be stressed that the MI coefficient is obtained for the first variation with respect to the dielectric tensor and is thus an estimate of the MI effect at frequency Ω only. A clear correspondence is found with the numerical results in figures 3 and 4, i.e. formula (4) for the MI effect correctly gives the linear contribution at frequency Ω. On figure 5, four elastic modes with the largest modulation coefficients can be identified, those with numbers 3, 6, 12, and 20.

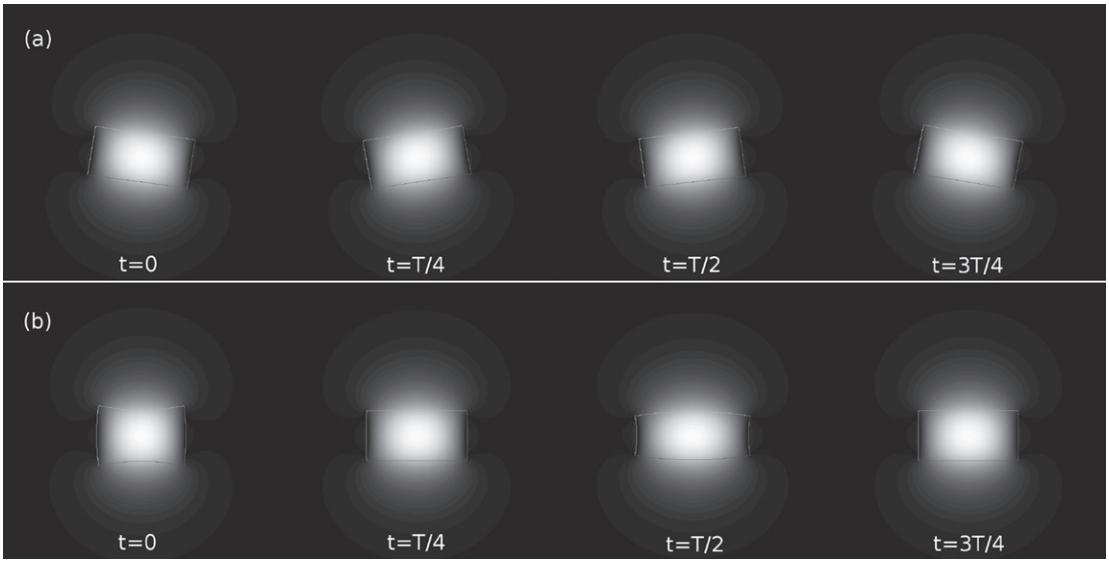

Figure 3. Variation of the fundamental TE optical mode inside an acoustic period for elastic modes number (a) 2 and (b) 3. The rectangular silicon nanowire waveguide is depicted in figure 2 and the wavelength in a vacuum $\lambda = 1550$ nm. The normalized $|H_y|$ component is depicted with a grey scale ranging from 0 (black) to 1 (white). Please note that the depicted modal displacements (see table 1) are much larger than the typical displacements in backward Brillouin scattering experiments.

Table 1. Maximum total displacement and symmetry properties of some elastic modes of the rectangular silicon nanowire waveguide of figure 2. The maximum total displacement is given for modes normalized so that $L_e = 0.1$ J. With respect to the horizontal axis (Ox) and the vertical axis (Oy), modes are either symmetric (S) or antisymmetric (AS).

Mode number	Max. $\|u\|$ (nm)	Sym./Ox			Sym./Oy		
		u_1	u_2	u_3	u_1	u_2	u_3
2	57	AS	S	AS	S	AS	AS
3	49	S	AS	S	AS	S	S
4	48	S	AS	S	S	AS	AS
6	23	S	AS	S	AS	S	S
12	14	S	AS	S	AS	S	S
20	15	S	AS	S	AS	S	S

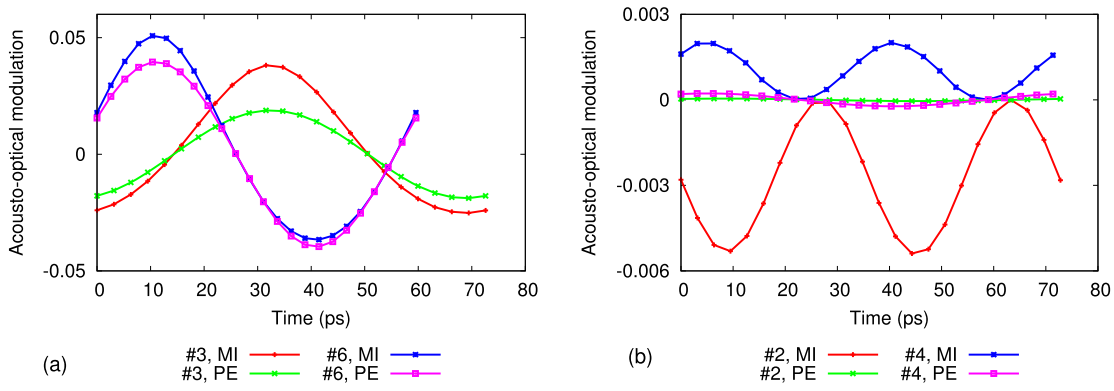

Figure 4. Variation of the relative acousto-optical frequency modulation ($\delta\omega/\omega$) caused by the moving-interface (MI) effect and the photoelastic (PE) effect, for elastic modes (a) number 3 and 6, and (b) number 2 and 4. The rectangular silicon nanowire waveguide is depicted in figure 2 and the wavelength in a vacuum $\lambda = 1550$ nm. The maximum total displacement and the symmetry properties of the considered elastic modes are listed in table 1.

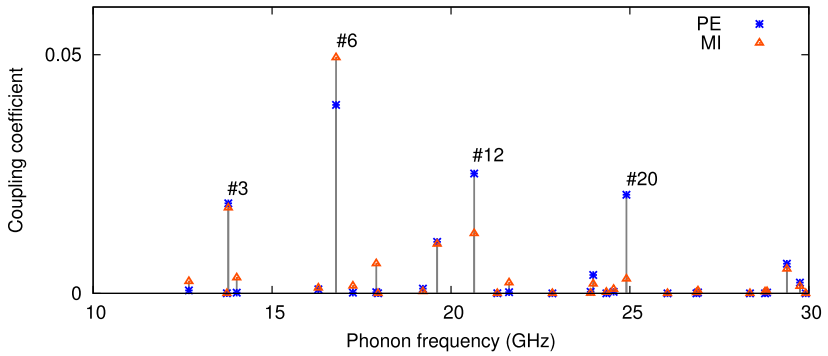

Figure 5. Absolute values of the photoelastic (PE) and moving-interface (MI) modulation coefficients $|\delta\omega/\omega|$ estimated using formulas (3) and (4) for all 29 elastic modes. Numbers on the main peaks refer to elastic mode numbers. The rectangular silicon nanowire waveguide is depicted in figure 2 and the wavelength in a vacuum $\lambda = 1550$ nm. The maximum total displacement and the symmetry properties of the elastic modes are listed in table 1.

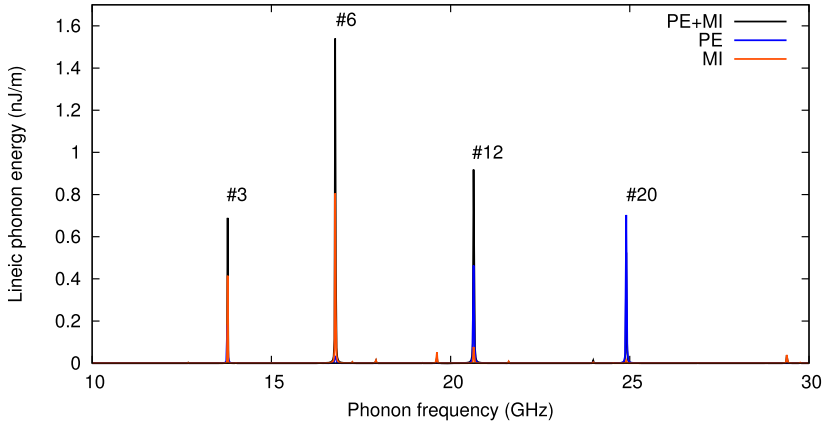

Figure 6. Lineic total elastic (or phonon) energy originating from electrostriction in the waveguide of figure 2. Two counter-propagating guided optical waves with unit power are assumed to be incident. The phonon frequency is determined by the detuning frequency Ω between the two optical waves. The individual and added contributions of the photoelastic (PE) and moving-interface (MI) effects are presented. Numbers on the main peaks refer to elastic mode numbers. A logarithmic scale version of this graph can be found in the supplementary material.

3.2. Surface and bulk electrostriction

From the previous numerical results, we are comforted with the idea that the contour integral term in the Lagrangian (12) is indeed representative of the MI effect at frequency Ω. We can now proceed to solve the boundary value problem (14), the solution of which ultimately gives the elastodynamic response of the waveguide subjected to the combined bulk optical stress and surface optical pressure. For that purpose, we again use the finite element method. Introducing test functions v_i, the weak form of (14) is obtained after application of the divergence theorem to transfer a partial derivative on the test functions as

$$-\Omega^2 \int_S \mathrm{d}S \rho v_i u_i + \int_S \mathrm{d}S v_{i,j} c_{ijkl} u_{k,l} = \int_S \mathrm{d}S v_{i,j} T_{ij}^{\mathrm{es}} + \int_\Sigma v_n \mathrm{d}l\, F_s, \tag{15}$$

an equation that is valid for all considered test functions. The bulk electrostriction stress term had already been obtained before [16, 17] but is here derived on a firmer ground from the Lagrangian. The electrostriction pressure term was absent from our previous works. The weak formulation (15) of the electrostriction process lends itself easily to implementation in a finite element code. It is here presented in the frame of waveguide problems, but it applies to cavity problems as well, the main difference being the presence or not of the acoustic wavenumber K.

The results presented in figure 6 assume that two guided optical waves with unit power and opposite wavevectors are propagating in the waveguide. The acoustic wavenumber is then $K \approx 2k^{(1)}$ as before. Because of phase matching, the detuning frequency Ω is also the phonon frequency. The total phonon energy is plotted as a function of Ω by considering either only bulk electrostriction (the photoelastic contribution), or only radiation pressure (the MI contribution), or both. As a note, viscoelastic damping in silicon is included in the computation by adding a frequency-dependent imaginary complex term to the elastic tensor [17, 27]. Sharp resonant peaks

are observed, each associated with a previously identified elastic mode. For the first two peaks, around the natural frequencies of modes number 3 and 6, the PE and MI contributions are of the same order of magnitude. For the two peaks at higher frequencies, around the natural frequencies of modes number 12 and 20, the PE contribution dominates over the MI contribution. Both contributions are found to interfere constructively to form the total electrostriction response.

4. Discussion

We have shown in the previous sections that both Brillouin scattering and electrostriction of phonons by light can be described by a single Lagrangian, from which the dynamical equations for optical and acoustic waves can be directly derived. Kroll had already undertook such a program back in 1965 [28], soon after SBS had been discovered [29]. His Lagrangian was also the sum of an optical and of an acoustic Lagrangian, complemented with an interaction Lagrangian. Only plane waves were considered and acousto-optical interaction was limited to the photoelastic effect, i.e. surface effects were not considered. Recently, Wolff *et al* also derived a Lagrangian to describe SBS in integrated photonic waveguides [15]. The independent optical variables in their Lagrangian are, however, different from ours, as they consider the electric and magnetic fields directly instead of the potentials in our formulation. They also do not make use of the total Lagrangian to derive dynamical equations, but to give a firm ground to the evaluation of coupling coefficients as overlap integrals of the form (3) and (4) and to argue that the energy that appears as mechanical work per acoustic cycle is precisely the change in the average optical energy density. The latter result also follows from the form of our Lagrangian (12), by construction, since we have added interaction terms to the Lagrangian as perturbations to the EM energy as caused by acoustic motion. In this sense, our results are complementary.

We have also obtained that the MI overlap integral approach applies only in the limit of neglecting processes other than one-phonon processes. It remains that under strong acoustic excitation such nonlinear effects could be observable in nanoscale waveguides. Using an external source or transducer for acoustic waves, it would probably be necessary to reach very high phonon energy densities for the phenomenon to be noticeable. In all-optical experiments such as SBS, however, there may be a possibility that the acoustic wave grows sufficiently intense, but this has not been observed so far to the best of our knowledge.

We had previously considered electrostriction in optical fibres [16] and waveguides [17], but without taking into account surface effects. In the particular example we have considered, the transverse dimensions of the waveguide were intently chosen sufficiently small that the MI effect would become comparable to the bulk photoelastic effect. In usual optical fibres and also in most microstructured optical fibres, it can be expected that bulk effects are dominant over surface effects, because of the involved dimensions. In the case of micro-fibres with small cores, however, surface contributions have been shown to be present [4] and must thus be taken into account for the smallest cores.

Overall, when the aim is to obtain coupling coefficients between coupled waves, it is an underlying assumption that the acoustic wave is a mode [30]. In our approach to electrostriction, the acoustic wave is generally not a mode but the solution to the forced elastodynamic equation [10, 16]: it depends on the driving bulk optical stress and optical pressure. The phonon distribution that we obtain is as a consequence different from a mere single mode, though it could still be expressed as a superposition of all available modes [16]. In the response shown in figure 6, for instance, only at frequencies corresponding to a strong peak does the phonon distribution approach that of a particular dominant elastic mode.

Furthermore, previous works had envisioned the possibility of an optical radiation pressure causing the boundaries of the waveguide to deform and hence to participate in the generation of the acoustic wave [10, 11]. This optical radiation pressure is clearly perfectly coherent with the bulk optical stress, having the same frequency and wavenumber. If one accepts that bulk electrostriction is the dual effect to the photoelastic effect, then one should also admit that radiation pressure is the dual of the moving interface effect, as was shown by Wolff *et al* based on thermodynamic arguments [15]. This duality is explicitly contained in the form of the Lagrangian (12).

5. Conclusion

In this paper, we have contributed to the modelling of the interaction of light and sound in optical waveguides. We have specifically investigated the MI contribution to Brillouin scattering and have shown that it is inherently nonlinear, leading to multi-phonon processes for large deformations. We have then proposed a total Lagrangian describing the interaction of sound and light, formed by summing the unperturbed optical and elastic wave Lagrangians with an interaction Lagrangian containing the first-order perturbation of the dielectric tensor. The total Lagrangian contains both surface and bulk contributions to Brillouin scattering and electrostriction, and

allows the derivation of optical and acoustic equations in a single variational formula. It also evidences clearly the duality of photoelasticity and bulk electrostriction, on the one hand, and of the MI effect and radiation pressure, on the other hand. A full electrostriction equation was then derived for the phonon distribution in the waveguide, with both bulk and surface effects included. Numerical simulations in the case of a silicon nanowire were used to illustrate the different effects and their respective contributions. For the dimensions chosen, the MI and the photoelastic contributions to both Brillouin scattering and electrostriction were found to be of comparable order of magnitude, in accordance with previous theoretical [10] and experimental [7, 8] observations. One salient aspect of the proposed model of electrostriction is that it avoids specifying the acoustic wave as a mode of the waveguide, but instead derives precisely the phonon distribution generated by the bulk optical stress and the optical pressure. For a complete description of SBS, and as a perspective, this phonon distribution could be inserted back in the optical coupled-wave equations to derive the exact Brillouin gain [10].

Acknowledgments

This work was supported by the OASIS project (ANR-14-CE36–0005-01) and the LABEX ACTION program (ANR-11-LABX-0001–01). Numerical implementation was performed using the finite element program FreeFem++ [31].

Appendix A. EM lagrangian

The derivation of the EM Lagrangian for the microscopic Maxwell's equations is well known but will be useful for the derivation of the macroscopic version. Let us rewrite (8) in tensor form

$$\mathcal{L}_o = -\rho_e \phi + j_i A_i + \frac{1}{2}\left(\epsilon_0 E_i E_i - B_i B_i/\mu_0\right) \tag{A.1}$$

and express the components of the electric and magnetic field vectors

$$B_i = e_{ijk} A_{j,k} \tag{A.2}$$

$$E_i = -\phi_{,i} - \dot{A}_i, \tag{A.3}$$

where e_{ijk} is the permutation tensor. The Euler–Lagrange equation obtained by variation with respect to ϕ gives Gauss' law at once

$$\rho_e = \epsilon_0 E_{i,i}, \tag{A.4}$$

while variation with respect to A_i leads to Ampère's law

$$j_i = -\epsilon_0 \dot{E}_i - \frac{\partial}{\partial x_j}\left(\frac{1}{\mu_0} e_{kij} B_k\right) = -\epsilon_0 \dot{E}_i + \frac{1}{\mu_0}(\nabla \times \boldsymbol{B})_i, \tag{A.5}$$

where the antisymmetric property of the permutation tensor has been used in the last transformation. As a whole, it is seen that the usual microscopic Maxwell's equations are derived from the Lagrangian as Euler–Lagrange equations.

We next consider the macroscopic form of Maxwell's equations and rewrite the Lagrangian (11) in tensor form

$$\mathcal{L}_o = \frac{1}{2}\left(E_i \epsilon_{ij} E_j - \frac{1}{\mu_0} B_i B_i\right). \tag{A.6}$$

By following the same rationale as in the microscopic case, the Euler–Lagrange equations are

$$0 = \left(\epsilon_{ij} E_j\right)_{,i} = \nabla \cdot \boldsymbol{D}, \tag{A.7}$$

$$0 = -\frac{\partial\left(\epsilon_{ij} E_j\right)}{\partial t} + \frac{1}{\mu_0}(\nabla \times \boldsymbol{B})_i = -\dot{D}_i + (\nabla \times \boldsymbol{H})_i, \tag{A.8}$$

or the macroscopic versions of Gauss' law and Ampères law. Again, it can be concluded that the usual macroscopic Maxwell's equations are derived from the Lagrangian as Euler–Lagrange equations.

The EM Hamiltonian can now be derived from the Lagrangian by a Legendre transform. The generalized momenta are defined as

$$\frac{\partial \mathcal{L}_o}{\partial \dot{\phi}} = 0, \tag{A.9}$$

$$\frac{\partial \mathcal{L}_o}{\partial \dot{A}_i} = -\epsilon_{ij} E_j = -D_i. \tag{A.10}$$

The Hamiltonian density is then

$$\begin{aligned}
\mathcal{H}_o &= \left(\dot{\phi}, \dot{A}_i\right) \cdot \left(0, -D_i\right) - \mathcal{L}_o, \\
\mathcal{H}_o &= -\dot{A}_i D_i - \mathcal{L}_o, \\
\mathcal{H}_o &= \phi_{,i} D_i + \boldsymbol{E} \cdot \boldsymbol{D} - \mathcal{L}_o, \\
\mathcal{H}_o &= \phi_{,i} D_i + \frac{1}{2}(\boldsymbol{E} \cdot \boldsymbol{D} + \boldsymbol{B} \cdot \boldsymbol{H}).
\end{aligned}$$

Except for the first term, this is the result we announced in section 2.3. Now since

$$\int_V \mathrm{d}V \phi_{,i} D_i = -\int_V \mathrm{d}V \phi D_{i,i} = 0, \tag{A.11}$$

the Hamiltonian is finally

$$H_o = \int_V \mathrm{d}V \frac{1}{2}(\boldsymbol{E} \cdot \boldsymbol{D} + \boldsymbol{B} \cdot \boldsymbol{H}). \tag{A.12}$$

Appendix B. Variation for an eigenvalue problem

Modal problems for wave equations can generally be cast under the form of a generalized eigenvalue problem

$$A\ |x\rangle = \omega^2 B\ |x\rangle, \tag{B.1}$$

where A and B are square matrices. If the matrices are varied by amounts δA and δB, then there are corresponding variations in the eigenvalue $\delta\omega$ and eigenvector $|\delta x\rangle$. Limiting the expansion to first order terms only (i.e., the first variation), we have

$$\delta A\ |x\rangle + A|\delta x\rangle \approx 2\omega\delta\omega B\ |x\rangle + \omega^2 \delta B\ |x\rangle + \omega^2 B|\delta x\rangle. \tag{B.2}$$

For lossless materials, matrix B is real symmetric, while matrix A is generally Hermitian. Their left- and right-eigenvectors are then complex conjugates and we obtain

$$\delta\omega \approx \frac{1}{2\omega} \frac{\langle x|\ \delta A\ |x\rangle - \omega^2 \langle x|\ \delta B\ |x\rangle}{\langle x|\ B\ |x\rangle} = \frac{\omega}{2} \frac{\langle x|\ \delta A\ |x\rangle - \omega^2 \langle x|\ \delta B\ |x\rangle}{\langle x|\ A\ |x\rangle}. \tag{B.3}$$

Formulas (3) and (4) for the coupling coefficients are obtained from the optical mode equation (5). In this particular case, A is a constant matrix, so that $\delta A = 0$, and $B = \epsilon$ so that $\delta B = \delta\epsilon$.

Appendix C. Euler–Lagrange equations in the case of mechanical loss

The case of mechanical loss can be encompassed by considering a dissipation function in addition to the elastic Lagrangian density. Following Landau and Lifshitz [24], the general form of a dissipation function describing internal friction in a deformed body is the quadratic form

$$\mathcal{R} = \mu_{ijkl} \dot{u}_{i,j} \dot{u}_{k,l} \tag{C.1}$$

with μ_{ijkl} the phonon viscosity tensor. This quadratic form cannot be incorporated in the elastic Lagrangian density since friction forces are not conservative. The dynamical equations are instead obtained from the following generalized Euler–Lagrange equations

$$\frac{\partial}{\partial t}\frac{\partial \mathcal{L}_e}{\partial \dot{u}_i} + \frac{\partial}{\partial x_j}\frac{\partial \mathcal{L}_e}{\partial u_{i,j}} - \frac{\partial}{\partial x_j}\frac{\partial \mathcal{R}}{\partial \dot{u}_{i,j}} = 0. \tag{C.2}$$

Given the expressions (7) and (C.1), the dynamical equations for purely elastic motion are

$$\rho \ddot{u}_i - \frac{\partial}{\partial x_j}\left(c_{ijkl} u_{k,l}\right) - \frac{\partial}{\partial x_j}\left(\mu_{ijkl} \dot{u}_{k,l}\right) = 0. \tag{C.3}$$

In case the displacements are caused by a time-harmonic elastic wave with angular frequency Ω, the previous equation simplifies to

$$\rho \ddot{u}_i - \frac{\partial}{\partial x_j}\left(\left[c_{ijkl} + \imath\Omega\mu_{ijkl}\right] u_{k,l}\right) = 0. \tag{C.4}$$

As a consequence, the elastic tensor becomes complex-valued with a frequency-dependent imaginary part proportional to the phonon viscosity tensor. This complex elastic tensor can be used in the elastodynamic

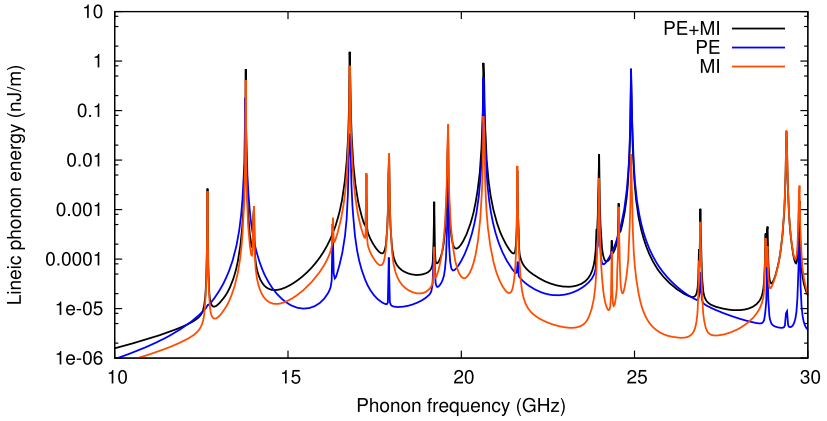

Figure D1. Lineic total elastic (or phonon) energy originating from electrostriction in the waveguide of figure 2. Two counter-propagating guided optical waves with unit power are assumed to be incident. The phonon frequency is determined by the detuning frequency Ω between the two optical waves. The individual and added contributions of the photoelastic (PE) and moving-interface (MI) effects are presented.

equation (14) to account for mechanical losses. Alternatively, the dynamical equations for the elastic wave generated by electrostriction and radiation pressure are

$$\rho\ddot{u}_i - \frac{\partial}{\partial x_j}\left(c_{ijkl}u_{k,l}\right) - \frac{\partial}{\partial x_j}\left(\mu_{ijkl}\dot{u}_{k,l}\right) + \frac{\partial}{\partial x_j}T_{ij}^{\mathrm{es}} = 0, \tag{C.5}$$

again complemented with the boundary condition that the optical pressure F_s applies on every boundary where the dielectric tensor is discontinuous.

Appendix D. Figure 6 plotted in logarithmic scale

Figure D1 shows the same information as figure 6, but with the phonon energy plotted with a logarithmic scale instead of a linear scale.

References

[1] Brillouin L 1922 *Ann. Phys.* **17** 21
[2] Boyd R W 2008 *Nonlinear Optics* 3rd edn (New York: Academic)
[3] Dainese P, Russell P, Joly N, Knight J, Wiederhecker G, Fragnito H, Laude V and Khelif A 2006 *Nat. Phys.* **2** 388–92
[4] Beugnot J C, Lebrun S, Pauliat G, Maillotte H, Laude V and Sylvestre T 2014 *Nat. Commun.* **5** 5242
[5] Pant R, Poulton C G, Choi D Y, Mcfarlane H, Hile S, Li E, Thevenaz L, Luther-Davies B, Madden S J and Eggleton B J 2011 *Opt. Express* **19** 8285–90
[6] Pant R, Byrnes A, Poulton C G, Li E, Choi D Y, Madden S, Luther-Davies B and Eggleton B J 2012 *Opt. Lett.* **37** 969–71
[7] Shin H, Qiu W, Jarecki R, Cox J A, Olsson R H III, Starbuck A, Wang Z and Rakich P T 2013 *Nat. Commun.* **4** 1944
[8] Van Laer R, Kuyken B, Van Thourhout D and Baets R 2015 *Nat. Photonics* **9** 199–203
[9] Rakich P T, Davids P and Wang Z 2010 *Opt. Express* **18** 14439–53
[10] Rakich P T, Reinke C, Camacho R, Davids P and Wang Z 2012 *Phys. Rev.* X **2** 011008
[11] Van Laer R, Kuyken B, Van Thourhout D and Baets R 2014 *Opt. Lett.* **39** 1242–5
[12] Aspelmeyer M, Kippenberg T J and Marquardt F 2014 *Rev. Mod. Phys.* **86** 1391
[13] Pennec Y, Laude V, Papanikolaou N, Djafari-Rouhani B, Oudich M, El Jallal S, Beugnot J C, Escalante J M and Martínez A 2014 *Nanophotonics* **3** 413–40
[14] Psarobas I E, Papanikolaou N, Stefanou N, Djafari-Rouhani B, Bonello B and Laude V 2010 *Phys. Rev.* B **82** 174303
[15] Wolff C, Steel M J, Eggleton B J and Poulton C G 2015 *Phys. Rev.* A **92** 013836
[16] Beugnot J C and Laude V 2012 *Phys. Rev.* B **86** 224304
[17] Laude V and Beugnot J C 2013 *AIP Adv.* **3** 042109
[18] Royer D and Dieulesaint E 1999 *Elastic Waves in Solids* (New York: Wiley)
[19] Johnson S G, Ibanescu M, Skorobogatiy M, Weisberg O, Joannopoulos J and Fink Y 2002 *Phys. Rev.* E **65** 066611
[20] Laude V, Escalante J M and Martínez A 2013 *Phys. Rev.* B **88** 224302
[21] El-Jallal S, Oudich M, Pennec Y, Djafari-Rouhani B, Laude V, Beugnot J C, Martínez A, Escalante J M and Makhoute A 2013 *Phys. Rev.* B **88** 205410
[22] Rolland Q, Oudich M, El-Jallal S, Dupont S, Pennec Y, Gazalet J, Kastelik J C, Leveque G and Djafari-Rouhani B 2012 *Appl. Phys. Lett.* **101** 061109
[23] Laude V, Khelif A, Benchabane S, Wilm M, Sylvestre T, Kibler B, Mussot A, Dudley J M and Maillotte H 2005 *Phys. Rev.* B **71** 045107
[24] Landau L D and Lifshitz E M 1975 *Theory and Elasticity* (*Course of Theoretical Physics* vol 7) 3rd edn (Oxford: Pergamon)

[25] Cohen-Tannoudji C, Dupont-Roc J and Grynberg G 1997 *Photons and Atoms: Introduction to Quantum Electrodynamics* (New York: Wiley)
[26] Wolff C, Steel M J and Poulton C G 2014 *Opt. Express* **22** 32489–501
[27] Helme B G and King P J 1978 *Phys. Status Solidi* a **45** 33–7
[28] Kroll N M 1965 *J. Appl. Phys.* **36** 34–43
[29] Chiao R Y, Townes C H and Stoicheff B P 1964 *Phys. Rev. Lett.* **12** 592–5
[30] Qiu W, Rakich P T, Shin H, Dong H, Soljačić M and Wang Z 2013 *Opt. Express* **21** 31402–19
[31] Hecht F 2012 *J. Numer. Math.* **20** 159–344